

## Topical Review

# Revealing the initial steps in homogeneous photocatalysis by time-resolved spectroscopy

Ayla Pöpcke, Aleksey Friedrich and Stefan Lochbrunner<sup>✉</sup>

Institute for Physics and Department of Life, Light and Matter, University of Rostock, 18051 Rostock, Germany

E-mail: [stefan.lochbrunner@uni-rostock.de](mailto:stefan.lochbrunner@uni-rostock.de)

Received 5 August 2019, revised 15 November 2019

Accepted for publication 4 December 2019

Published 9 January 2020

**Abstract**

Photocatalysis attracts currently intense research since it can provide efficient routes for generating solar fuels and allows to apply sunlight for an environmentally friendly synthesis of valuable chemical compounds. Accordingly, in future photocatalysis may contribute significantly to a sustainable economy. However, up to now photocatalysis has made it only into some niche applications. The reasons are manifold including too low yields, insufficient stability, and scarce availability of the precious metals and rare earths used in most cases. The design of better systems is the goal of many research activities. They call for a detailed knowledge of the individual steps and the microscopic mechanisms.

Time-resolved spectroscopy is a powerful tool to improve our understanding of the individual steps of a photocatalytic process and of the efficiencies and losses associated with them. This allows to address specific weaknesses of the components of a photocatalytic system and to pursue a rational design of the corresponding compounds. In this review an overview is given about what insights can be gained by time-resolved spectroscopy referring mostly to our own results while it has to be stressed that many other groups are also highly successfully working in this area. We restrict ourselves to homogeneous systems which are often easier to analyze and focus on the primary steps occurring after optical excitation. This includes intramolecular relaxation and intersystem crossing in the photosensitizer as well as the first electron transfer step resulting from the interaction of the sensitizer with other components of the system. Ultrafast pump-probe spectroscopy turns out to be particularly helpful in analyzing new photosensitizers based on abundant metals, i.e. copper and iron. These sensitizers can suffer from short lifetimes of the metal-to-ligand charge transfer states which are typically involved in the intermolecular charge transfer processes. The latter are investigated on the pico- to microsecond timescale by quenching experiments making use of a streak camera and by pump-probe spectroscopy applying a YAG-laser system for excitation. The experiments with the streak camera allow to discriminate between oxidative and reductive pathways and to determine the corresponding bimolecular quenching rates which are compared to their diffusion limit to obtain a measure for the quenching efficiency. By applying transient absorption spectroscopy, it is furthermore possible to observe appearing charge transfer products and to determine their concentrations. In this way the efficiency of the electron transfer itself can be deduced and the relevance of lossy quenching events can be estimated.

Keywords: photocatalysis, photosensitizers, pump-probe spectroscopy, time-resolved luminescence, electron transfer

(Some figures may appear in colour only in the online journal)

## 1. Introduction

Currently, photocatalytic systems are intensively investigated since they hold the promise to make a significant contribution to a sustainable future economy [1–8]. Catalysis in general is studied and applied by an extremely large community and mechanistic investigations are of crucial importance for the design of the systems but also challenging due to the complexity of the involved processes [9, 10]. Photocatalysis allows to use sunlight as energy source in the synthesis of valuable chemicals and to produce solar fuels. A prototypical example for the latter is photocatalytic water splitting [11–14]. It is a promising approach to generate hydrogen which can then be used as fuel that provides energy without the generation of carbon dioxide which is mainly responsible for global warming. While nature is successfully producing hydrogen using sunlight and catalytic processes [15], photocatalytic systems are not yet applied for sustainable energy generation. The reasons are manifold and include too low yields, insufficient stability, and scarce availability of precious metals and rare earths [16]. To address some of these problems it would be most helpful to analyze the individual steps taking place in a photocatalytic system and to characterize their efficiencies and corresponding losses and competing channels. The gained knowledge can then be used to improve the design of the system and its components in a rational and targeted way. Time-resolved spectroscopy is a very powerful tool for this analysis [17, 18]. In particular, the steps occurring directly or shortly after an absorption event are well accessible by such techniques while other methods usually lack the necessary time resolution but are more suitable for the analysis of the subsequent proton dynamics and catalytic reactions. In the following we want to give an overview about what can be learned by time-resolved spectroscopy about the primary steps in photocatalysis. The review is confined to homogeneous systems, which are typically easier to analyze, and deals with the first electronic relaxation and electron transfer steps. It provides examples and topics mostly from our own work, however, it should be pointed out that many other groups are also very successfully applying time-resolved spectroscopy to photosensitizers and photocatalysis [19–21].

To introduce the typical setting and the roles, the different components of a photocatalytic system play, we discuss as an example shortly the system shown in figure 1. Usually the water reduction and the oxidation side of photocatalytic water splitting are investigated separately to simplify the problem. The here presented homogeneous system performs photocatalytic water reduction and was developed by Matthias Beller and coworkers. It is based on iridium or copper complexes as photosensitizers (PS) and the iron complex  $[\text{HFe}_3(\text{CO})_{11}]^-$  as water reduction catalyst [22, 23]. The electrons needed

for the reduction process result ultimately from a sacrificial electron donor, in the present example triethylamine (TEA). However, without additional energy, the electrons cannot be transferred from the donor to the catalyst, since the accepting orbital of the catalyst must have a strong reduction power to reduce protons present in the solution to molecular hydrogen. Accordingly, it exhibits a rather high energy contrary to the highest occupied molecular orbital (HOMO) of the donor. The PS delivers the energy needed for the transfer and provides electrons with a sufficiently negative reduction potential to be used by the catalyst. The energy is supplied by the photons absorbed by the PS. An absorption event typically results, maybe after a fast electronic relaxation step, in the population of the first electronically excited state in which an electron is promoted from the HOMO to the lowest unoccupied molecular orbital (LUMO) of the PS. The excited electron exhibits a strong reduction potential and can be transferred to the catalyst while the hole in the HOMO can accept the electron from the sacrificial donor completing the transfer cascade.

Many metal complexes exhibit long-lived metal-to-ligand charge transfer (MLCT) states which make them particularly suitable as PSs. These states are characterized by the transfer of an electron from a d orbital of the metal ion, which is at the same time the HOMO of the complex, to a  $\pi^*$  orbital of the ligand, which is typically the LUMO of the complex. Transitions from the electronic ground state to MLCT states with the same multiplicity are usually responsible for the lowest electronic absorption band of the PS which is located in the visible or near ultraviolet region. Absorption of light leads after intersystem crossing and electronic relaxation to the population of long-lived triplet MLCT states. The states are redox active since the extra electron on the ligand has a strong reduction power while the generated hole at the metal acts oxidizing. After optical excitation of the PS two reactive routes are potentially feasible. The system can take a reductive path and the excited PS accepts an electron from the sacrificial donor oxidizing the latter. The extra electron of the ligand is only in a second step transferred to the catalyst which then performs the reduction of protons. Or the oxidative route is taken and first the excited electron is transferred to the catalyst, resulting in an oxidized PS. The latter is in a second step reduced back to its original ground state by an electron transfer from the sacrificial donor while in parallel the reduced catalyst is involved in hydrogen generation.

The proton dynamics associated with the generation of molecular hydrogen is not subject of the investigations discussed in this article but was studied by operando methods such as NMR and *in situ* FTIR spectroscopy [14] and is sketched here for completeness. In that specific case the photosensitizer was an iridium complex. However, the proton dynamics itself should be similar for the various sensitizers. The studies

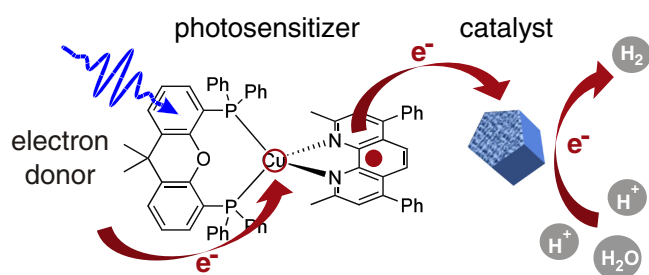


**Figure 1.** Scheme of a homogeneous photocatalytic system for water reduction and the role of the photosensitizer thereby.

point to the following reaction scheme. Under light irradiation and in the presence of TEA, the interaction of the iron catalyst  $[\text{HFe}_3(\text{CO})_{11}]^-$  with an excited sensitizer molecule and the corresponding reductive electron transfer are supposed to yield  $[\text{HFe}_3(\text{CO})_{11}]^{2-}$ . This complex is then transformed by a subsequent protonation step to  $[\text{H}_2\text{Fe}_3(\text{CO})_{11}]^-$ , from which  $\text{H}_2$  is released resulting in  $[\text{Fe}_3(\text{CO})_{11}]^-$ . A further reduction by a second excited photosensitizer yields then  $[\text{Fe}_3(\text{CO})_{11}]^{2-}$ . From the latter  $[\text{HFe}_3(\text{CO})_{11}]^-$  is restored, again by protonation, and the cycle restarts [14, 24].

While the particular role of the catalyst described here is specific for a homogeneous water reduction system the electron transfer steps involving the PS appear also in many other applications like in dye sensitized solar cells and heterogeneous photocatalysis. In both cases the optically excited electron is injected into the conduction band of a semiconductor and the hole filled by an electron from the valence band.

From the described operation mode a number of requirements follows which have to be met by an efficient PS [25–29].

- (1) Its absorption spectrum should have a good overlap with the solar spectrum.
- (2) Its MLCT state must be redox-active, i.e. the involved metal orbital should have a high oxidation potential and the electron accepting orbital on the ligand a strong oxidation potential.
- (3) The above point implies that electronic relaxation steps after optical excitation should reduce the energy as little as possible.
- (4) The MLCT state has to be long-lived to allow for interaction with the other components of the system and the electron transfer steps to happen. Electronic relaxation back to the ground state or to low lying electronic states has to be slow.
- (5) The actual electron transfer steps should proceed with high yields and should not be compromised by electron back transfer.
- (6) The PS has to be stable in order to achieve large turnover numbers.

In order to assess the performance and the shortcomings of a specific PS and to understand their impact on the overall yield of a photocatalytic system all these aspects should be considered. Points (1), (2), (3), and (6) can be addressed

by stationary absorption spectroscopy and electrochemistry. However, points (4) and (5) call for time-resolved spectroscopic methods which allow to characterize electronic relaxation processes, even if they take place on ultrafast timescales, and to observe electron transfer events involving the PS.

In this review we describe by means of specific examples how time-resolved spectroscopy can be applied to photocatalytic systems to obtain insights into the electronic dynamics and to understand the reaction mechanisms and efficiency limiting factors. Several different spectroscopic techniques are used in order to cover a wide range of timescales. Intramolecular processes of the photosensitizers, which occur directly after absorption of a photon, are studied by femto-second pump-probe experiments since they are typically very fast. This includes electronic as well as structural relaxation processes, intersystem crossing and interligand charge transfer. The lifetimes of the electronically excited states are further characterized by recording their time dependent luminescence with a streak camera. The interaction between the sensitizer and other components of the system is investigated by analyzing the quenching of the photoluminescence due to this interaction. In an optimized system the interaction should lead to a complete electron transfer. To detect potential transfer products absorption measurements are carried out applying a YAG-laser system for excitation. Making use of an electronic delay generator allows to extend the time window of the transient absorption measurements to almost a millisecond.

Combining ultrafast pump-probe spectroscopy, time-resolved luminescence measurements, and transient absorption spectroscopy with nanosecond resolution allows to monitor and identify the steps occurring from the absorption of a photon by the photosensitizer till the intermolecular electron transfer between the sensitizer and the catalyst or the electron donor. The electron transfer to the catalyst in turn initiates a proton dynamics which finally results in the liberation of molecular hydrogen. However, with the methods discussed here these processes are difficult to access since they involve intermediates at very low concentrations, which are often associated with weak and unspecific optical signatures, and involve typically time scales beyond a millisecond. Here numerous other approaches have been already successfully applied including operando methods based on electron paramagnetic resonance, Raman scattering, and infrared spectroscopy [14, 30, 31].

In the following first the experimental methods for time-resolved spectroscopy are shortly introduced and then ultrafast pump-probe studies on copper and iron complexes discussed which shed light on the intramolecular relaxation processes of the complexes and provide valuable information for the design of the active electronic states. Subsequently quenching experiments on iridium and copper photosensitizers using time-resolved emission measurements are described and finally pump-probe experiments in the nano- and micro-second time range providing quantitative access to intermolecular electron transfer processes.

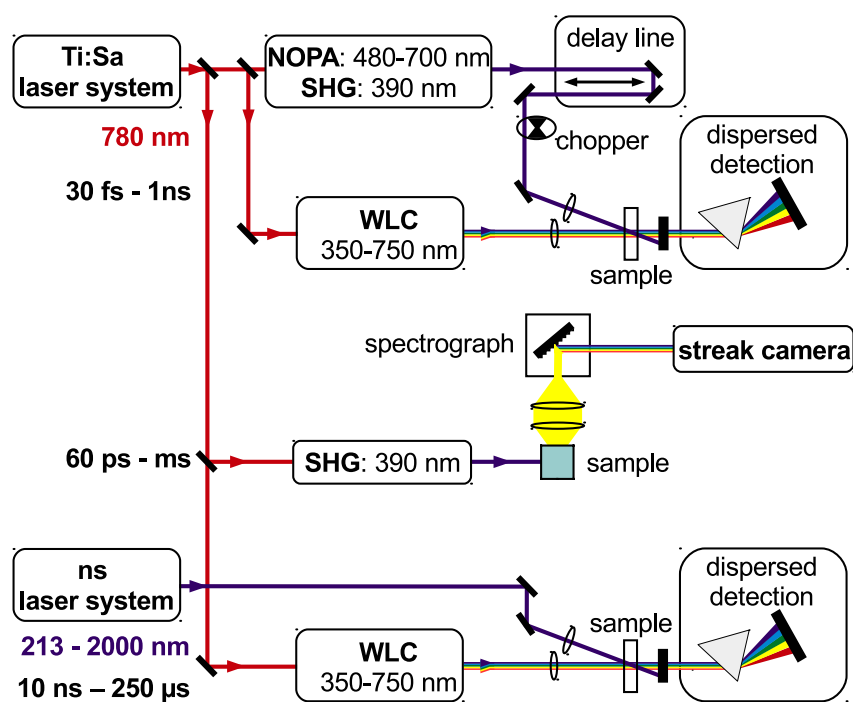


**Figure 2.** Schematic setups for ultrafast pump-probe measurements, time-resolved emission spectroscopy by a streak camera, and transient absorption spectroscopy on the nano- and microsecond timescale.

## 2. Experimental methods

Time-resolved optical spectroscopy is a powerful approach to investigate the various reaction steps occurring in a photocatalytic system [17, 18]. Pump-probe absorption spectroscopy is highly suitable to characterize intramolecular electronic relaxation as well as intermolecular charge transfer processes since different electronic or charge states exhibit usually different characteristic absorption bands in the spectral region from the near infrared to the ultraviolet. Combining this technique with time-resolved emission measurements allows to discriminate electronically excited states, which show typically some emission, from species in the ground state and to determine the lifetime of the excited states and the efficiency of quenching processes. However, the light induced processes in a photocatalytic system occur on very different timescales ranging from femtoseconds for intramolecular relaxation steps to microseconds for diffusion controlled reactions [17, 18, 32]. In order to cover all relevant timescales several experimental approaches have to be combined. Figure 2 shows schematically a set of spectroscopic experiments with which this goal is achieved.

### 2.1. Transient absorption measurements

Transient absorption spectra are recorded by pump-probe measurements [33, 34]. A short laser pulse with a wavelength at which the targeted compound, e.g. a photosensitizer absorbs, excites a significant fraction of these molecules. The resulting changes in the absorption spectrum are probed at a specific time delay by a second laser pulse which passes through the sample after the pump. In the case of ultrafast experiments, the time delay is varied by changing the length

of the beam path for one of the pulses using a retroreflector mounted on a motorized and computer controlled linear stage, see figure 2. For measurements on timescales longer than single nanoseconds the delay time can be controlled directly by electronic means [17]. To this end the pump and probe pulses are generated by two different laser systems which are fired at suitable times by a trigger and delay generator.

In the ultrafast measurements typically a regenerative Ti:sapphire laser system with a centre wavelength of about 800 nm and a repetition rate in the kilohertz range is used as primary source of the laser pulses. Its output is split into a weak probe and stronger pump beam. The probe pulses should have a broad spectrum which allows to monitor the absorption changes in a wide spectral window. Therefore a white light continuum (WLC) is usually applied for this purpose which is generated by focusing the weak Ti:sapphire pulses into a  $\text{CaF}_2$ -substrate [34, 35]. The resulting continuum can cover the whole visible and the near ultraviolet spectral region. Pump pulses with a centre wavelength of about 400 nm are obtained by frequency doubling (second harmonic generation, SHG) the near infrared pulses of the laser system in a beta barium borate (BBO) crystal. Pump pulses in the visible are generated from the NIR pulses by non-collinear optical parametric amplifiers (NOPA) [36, 37]. Pulse durations below 20 fs can be obtained if the dispersion of the setup is compensated, e.g. by a prism compressor. Pump and probe pulses are focused onto a common spot in the sample which is typically a solution in a 1 mm thick fused silica cell. The polarizations of the pump and probe pulses are usually set to magic angle relative to each other since in this case the pump induced anisotropy and orientational relaxation do not affect the signal [38]. After the sample the probe beam is spectrally dispersed by a prism



or a grating spectrograph and the spectrum of the probe pulses, which is modified by the sample absorption, is recorded by an array detector. To correct for fluctuations of the probe spectrum the pump is blocked every other shot by a chopper and probe spectra  $I_{\text{probe}}^*(\lambda, t)$  and  $I_{\text{probe}}^0(\lambda, t)$  are recorded with and without pump directly after each other. From these spectra the wavelength and time dependent absorption change  $\Delta A(\lambda, t)$  induced by the pump pulses and the subsequent dynamics is calculated by  $\Delta A(\lambda, t) = -\lg(I_{\text{probe}}^*(\lambda, t)/I_{\text{probe}}^0(\lambda, t))$ . To achieve a good signal-to-noise ratio and a sensitivity for  $\Delta A$  of about  $5 \cdot 10^{-4}$  typically five time scans are performed and for every time point in each scan 200 probe spectra with and without pump pulse are recorded. The final data set is obtained by averaging the individual spectra as well as the scans.

The time resolution of the pump-probe setup depends on the probe wavelength and the sample thickness due to the dispersion of the solution. In the case of thin samples e.g. using a 100  $\mu\text{m}$  thick cell and if the probe wavelength coincides with the excitation wavelength the cross correlation between pump and probe pulses can be as short as 50 fs. If the sample is 1 mm thick and pump and probe wavelengths are spectrally well separated the cross correlation and thus the time resolution is typically 100 fs.

To extend the pump-probe scheme to timescales longer than single nanoseconds the pump pulses are generated by a separate laser system which is electronically synchronized with the femtosecond laser system, see figure 2. A YAG-laser system equipped with an optical parametric oscillator has proven to be a very versatile pump source providing tunable nanosecond pulses in the ultraviolet and visible spectral range [17, 23]. The probe pulse generation and the detection scheme are not changed and the recorded transient absorption spectra have the same properties as the ultrafast spectra. The time delay between pump and probe is adjusted and varied by an electronic trigger generator.

## 2.2. Time-resolved luminescence measurements

Time-resolved emission measurements are a sensitive and potent approach to determine the lifetimes of electronically excited states if they show at least somewhat fluorescence or phosphorescence [39, 40]. The optical excitation is done by short laser pulses, e.g. by the frequency doubled pulses from a Ti:sapphire laser system or the output of a NOPA, see figure 2. The resulting luminescence of the sample is dispersed by a grating spectrograph and its time depend intensity recorded by a fast detector. Often time-correlated single photon counting (TCSPC) is performed using a fast photomultiplier or avalanche photodiode as detector [41]. An attractive alternative is a streak camera since it features an array detector and allows to record the whole emission spectrum and its time evolution in a single experimental run while in TCSPC only a single signal trace is obtained [22]. Both methods are very sensitive, provide a time-resolution typically in the order of a few ten picoseconds, and cover at the same time also very long timescales only limited by the lifetime of the emitter.

## 3. Intramolecular relaxation in metal complexes used as photosensitizers

The study of photosensitizers was primarily focusing on complexes featuring noble or rare earth metals such as platinum, ruthenium, iridium, and rhenium, with Ru(II) polypyridines and cyclometalated Ir(III) complexes being the most popular ones [42, 43]. These complexes perform as PSs quite well but the metals are very rare, expensive and accordingly not suitable for large scale applications such as light harvesting and photocatalytic synthesis of solar fuels. Research turns therefore more and more to complexes based on nonprecious metals like copper [44, 45] and iron [27, 46]. In the past, luminescent Cu(I) complexes were already used in various applications such as organic light-emitting diodes (OLEDs) [47–51]. A fully noble-metal-free system for photocatalytic hydrogen generation was reported in 2013 [52]. It makes use of a heteroleptic copper(I) photosensitizer (CuPS) in combination with the above introduced iron complex  $[\text{HFe}_3(\text{CO})_{11}]^-$  as water reduction catalyst. However, known copper and iron complexes still suffer from unfavorable photophysical properties such as bad overlap between absorption and solar spectrum or short lifetimes of the MLCT states. The latter issue is particularly severe in the case of iron. Several groups work on solving these problems [53–63]. To learn about the responsible mechanisms and to guide and validate synthetic strategies the intramolecular dynamics after an absorption event has to be characterized. To this end ultrafast time-resolved spectroscopy is the method of choice. In the following results of pump-probe measurements on copper and iron complexes are presented which were designed with the goal to improve their photophysical properties.

### 3.1. Copper complexes

In the photocatalytic experiments heteroleptic copper(I) photosensitizers of the type  $[(\text{P}^*\text{P})\text{Cu}(\text{N}^*\text{N})]^+$ , with a diimine  $\text{N}^*\text{N}$  and bulky diphosphine  $\text{P}^*\text{P}$  chelate ligand, result contrary to homoleptic  $[\text{Cu}(\text{N}^*\text{N})_2]^+$  complexes in high activities. Copper(I) complexes have a  $d^{10}$  valence configuration, i.e. the d subshell is completely filled. Accordingly, no excited ligand field states are present in complexes of this ion and the lowest electronically excited state is  $^3\text{MLCT}$  in nature [64]. Interestingly, the heteroleptic complexes possess longer  $^3\text{MLCT}$  lifetimes than the homoleptic analogs  $[\text{Cu}(\text{N}^*\text{N})_2]^+$ . This is attributed to a weaker geometrical distortion in the  $^3\text{MLCT}$  state of the former compared to the homoleptic complex due to their steric demanding diphosphine ligand [65–68]. It is suggested that the reduced distortion is beneficial for the activity of the PSs and might be responsible for the differences between the homo- and heteroleptic complexes.

To characterize the light induced intramolecular dynamics in photocatalytically active heteroleptic copper complexes the four compounds **Cu1–Cu4** shown in figure 3 were investigated by Tschierlei *et al* using ultrafast absorption spectroscopy [69]. All of them perform well as photosensitizer in photocatalytic hydrogen generation. They feature the

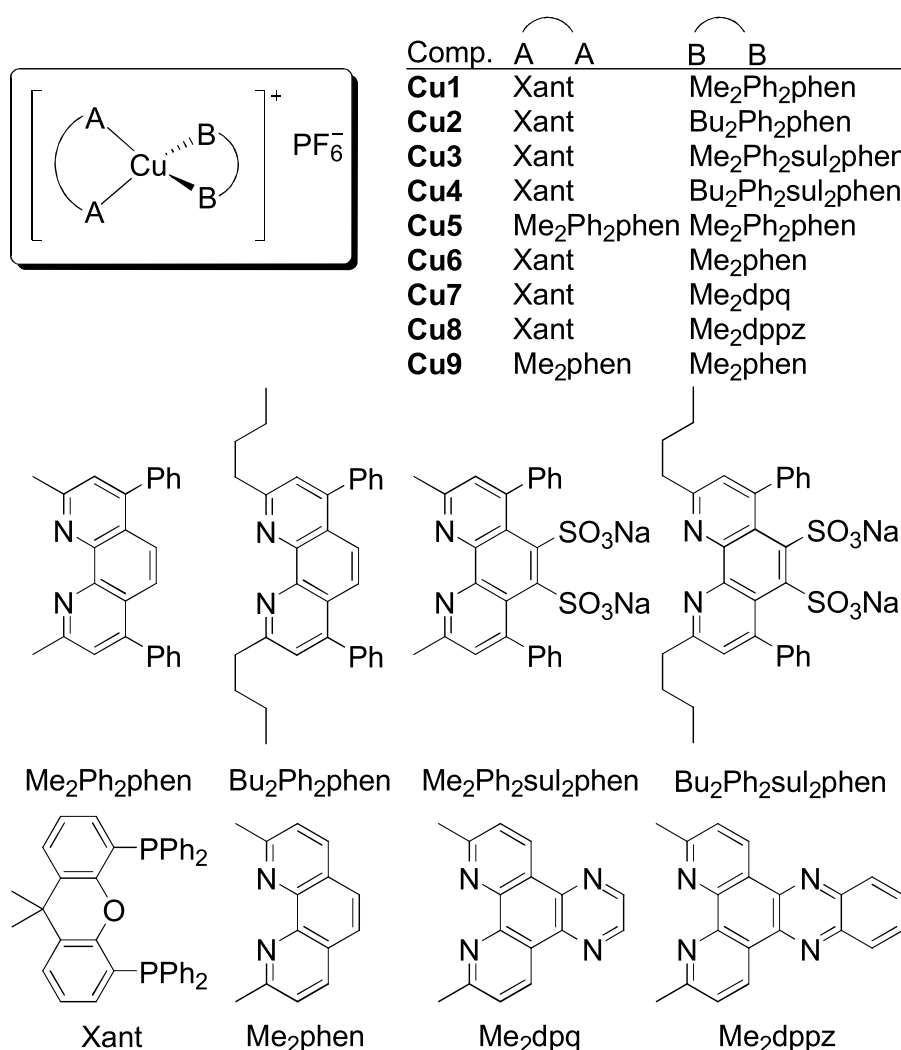


Figure 3. Considered copper complexes.

diphosphine ligand Xantphos (Xant) and a substituted phenanthroline (phen) ligand. Complexes **Cu3** and **Cu4** have two sulfonate groups (sul) substituted to the phenanthroline moiety which allows to link them to titanium dioxide substrates.

In the pump-probe measurements complexes **Cu1–Cu4**, dissolved in acetonitrile (ACN), were optically excited at 388 nm, i.e. in the absorption band of the MLCT transition. TDDFT calculations of **Cu1** revealed that this band with its maximum around 390 nm is due to the  $S_1 \leftarrow S_0$  transition which involves excitations from the copper d orbitals to the  $\pi^*$  orbital of the phenanthroline ligand [69]. Immediately after optical excitation of **Cu1** a broad absorption band covering almost the whole visible region up to 700 nm appears (figure 4). It exhibits two peaks at around 440 nm and 540 nm. The excited state absorption at 440 nm decreases during the first few tens of picoseconds while the second band rises parallel on the same timescale. The transient absorption spectra of complexes **Cu3** and **Cu4** exhibit a very similar evolution.

For a quantitative evaluation of the data a global fit is applied. The entire transient absorption change  $\Delta A(\lambda, t)$ , as a function of probe wavelength  $\lambda$  and delay time  $t$ , was fitted by a global multi-exponential function of the form  $F(\lambda, t) = \sum_i^N \text{DAS}_i(\lambda) \cdot \exp(-t/\tau_i) + \text{DAS}_\infty(\lambda)$ , where

$\text{DAS}_\infty$  is a long-living component. The spectral distribution of the decay component with the time constant  $\tau_i$  is described by its decay associated spectrum  $\text{DAS}_i$ . For all complexes **Cu1–Cu4**, two decay components ( $N = 2$ ) and the long-living one were sufficient to reproduce accurately the data. The shorter of the two time constants is in the order of 1 ps while the longer one in the range of 6 ps–8 ps [69]. The exact values are given in table 1.

Homoleptic bis-diimine copper complexes such as **Cu9** were investigated by various ultrafast spectroscopic techniques previously [70, 71]. A very similar dynamics was found even though they do not show any activity in the homogeneous photocatalytic system presented above [69, 72]. In the case of **Cu5** the fast step taking 0.7 ps is assigned to a ‘flattening’ of the complex structure from a pseudo-tetrahedral to a distorted square planar geometry and the second step with a time constant of 7.5 ps to intersystem crossing (ISC) from the singlet  $^1\text{MLCT}$  to the triplet  $^3\text{MLCT}$  state. This interpretation holds also in case of **Cu1–Cu4** and is supported by the variation of the time constants with the substituents [69]. The distortion process of homoleptic bis-diimine complexes takes place in about 0.7 ps, as already mentioned, while it is with  $\tau_1 = 1.0$  ps slightly slower in the heteroleptic complexes **Cu1**

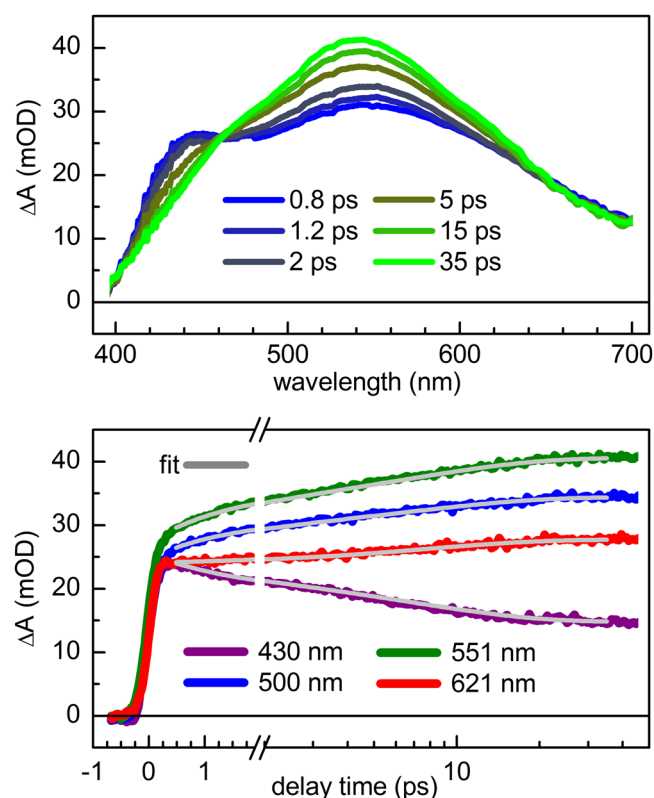


**Figure 4.** Transient absorption spectra (upper panel) and time traces at selected probe wavelengths (lower panel) for **Cu1** in ACN after optical excitation at 388 nm. Reproduced from [69]. John Wiley & Sons. © 2014 WILEY-VCH Verlag GmbH & Co. KGaA, Weinheim.

and **Cu2** (table 1). This slowdown is most likely caused by the much heavier and extended Xantphos ligand. In the case of **Cu3** and **Cu4** the distortion time increases further to 1.4 ps. This is attributed to the heavy sulfonate groups at the 4,5-position, which roughly double the molar weight of the phenanthroline ligand. The growth of  $\tau_1$  with mass and inertia of the ligands supports its assignment to the flattening of the complex structure. The second time constant  $\tau_2$  seems to be linked to the electronic properties of the substituents which is in line with its assignment to the ISC step [69]. The *n*-butyl groups result in a somewhat longer time for **Cu2** (8.4 ps) compared to **Cu1** (7.4 ps), which might be due to the slightly stronger electron donating effect of the *n*-butyl in comparison to the methyl substituents. The same trend is found concerning the sulfonate groups. Since this group has a strong electron withdrawing character the electron density at the phenanthroline ligand is decreased and, consequently, the ISC faster in compounds **Cu3** (6.5 ps) and **Cu4** (6.8 ps).

In summary, heteroleptic Cu(I) complexes exhibit after absorption of light fast relaxation steps which lead to population of the triplet MLCT state in less than 10 ps. The lifetime of this state in turn can range from some ten nanoseconds to several microseconds as time-resolved phosphorescence measurements show, see table 1. This behavior is similar to Ru and Ir complexes. Relaxation and ISC to the  $^3\text{MLCT}$  state are in these compounds even faster and can occur in less than 100 fs [74–76]. The  $^3\text{MLCT}$  lifetimes are of similar order of magnitude as in the Cu complexes. However, Ru and Ir complexes

**Table 1.** Time constants obtained from transient absorption measurements ( $\tau_1 - \tau_3$ ) and lifetimes of the  $^3\text{MLCT}$  state ( $\tau_{\text{MLCT}}$ ) for various Cu(I) complexes [69, 73].

Compound <sup>a</sup>	$\tau_1$ (ps)	$\tau_2$ (ps)	$\tau_3$ (ps)	$\tau_{\text{MLCT}}$ (ns)
<b>Cu1</b>	1.1	7.4	—	3500
<b>Cu2</b>	1.0	8.4	—	4700
<b>Cu3</b>	1.4	6.5	—	1900
<b>Cu4</b>	1.4	6.8	—	4300
<b>Cu5</b>	0.7	7.5	—	n.d. <sup>b</sup>
<b>Cu6</b>	0.9	8.9	—	64.0
<b>Cu7</b>	1.1	13.7	—	28.0
<b>Cu8</b>	0.9	8.7	130	14.5 <sup>c</sup>
<b>Cu9</b>	0.9	9.8	—	54.0

<sup>a</sup> Complexes **Cu1**–**Cu5** were measured in methanol, **Cu6**–**Cu9** in acetonitrile.

<sup>b</sup> n.d.: not determined because the emission was below the detection limit.

<sup>c</sup> Lifetime of the *dark* state, contrary to most other Cu complexes no emission is observed.

show typically a better performance as photosensitizers compared to corresponding Cu compounds. This is, at least to a large extent, related to the lower stability of the Cu complexes and their absorption spectra which extend from the ultraviolet only weakly into the visible region.

Since heteroleptic Cu(I) complexes still suffer from a limited absorption in the visible a red shift of their absorption spectrum is highly desirable. To this end a promising strategy is to extend the conjugated  $\pi$ -system of one of the ligands. Along this line heteroleptic complexes **Cu7** and **Cu8** featuring diimine ligands with an enlarged  $\pi$ -system, i.e. 3,6-dimethyldipyrido[3,2-*f*:2',3'-*h*]-quinoxaline (**Me<sub>2</sub>dpg**) and 3,6-dimethyldipyrido[3,2-*a*:2',3'-*c*]phenazine (**Me<sub>2</sub>dppz**), respectively were synthesized by Karnahl *et al* and their photophysical and -catalytic properties were compared to **Cu6** exhibiting the diimine ligand 2,9-dimethyl-1,10-phenanthroline (**Me<sub>2</sub>phen**) [73]. The diphosphine ligand of all complexes is again Xantphos. The effects on the absorption spectra were actually weak and only a slight increase of the molar extinction coefficient in the long wavelength wing around 450 nm was observed for the extended  $\pi$ -systems. Above all the photocatalytic activity was quite poor.

To understand the last point studies applying ultrafast pump-probe spectroscopy were performed [73]. While they found for **Cu6** and **Cu7** again a double exponential relaxation to a long-living transient absorption in **Cu8** three exponential decay components were observed, see table 1. The flattening from the distorted tetrahedral structure of the electronic ground state to a more square planar one takes in all cases again about 1 ps. ISC occurs within 8.9 ps in complex **Cu6** and 13.7 ps in **Cu7** which is in the same range as for similar heteroleptic CuPS, see above. In **Cu7** the ISC is decelerated compared to **Cu6** probably due to the extended  $\pi$ -system and the changed electron density at the phenanthroline moiety. In **Cu8**, ISC takes 8.7 ps and is similar fast than in **Cu6**. The similarity results probably from the fact that the acceptor orbital of the optically addressable MLCT state is mainly located on the phenanthroline part of the **Me<sub>2</sub>dppz** ligand (figure 1) and does not extend over the whole diimine ligand as in **Cu7**.

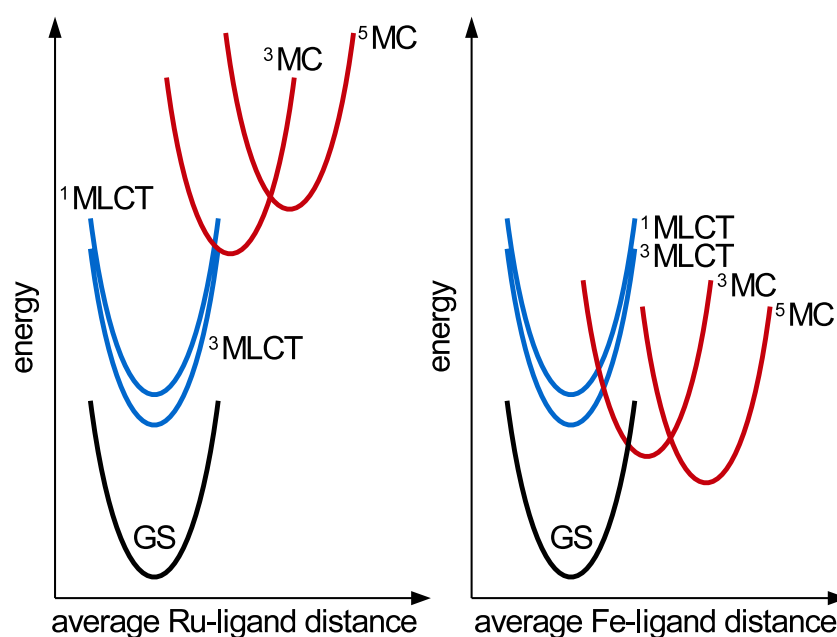


**Figure 5.** Schematic potential energy surfaces of the ground (GS, black), MLCT (blue) and MC states (red) for  $[\text{Ru}(\text{bpy})_3]^{2+}$  (left) and  $[\text{Fe}(\text{bpy})_3]^{2+}$  (right) [46].

Contrary to the other Cu complexes, for **Cu8** a third time constant of 130 ps was found [73]. It reflects the relaxation from the  $^3\text{MLCT}$  state populated by the ISC step to a lower lying  $^3\text{MLCT}$  state whose acceptor orbital is located on the phenazine part of the  $\text{Me}_2\text{dppz}$  ligand. Since there is practically no spatial overlap between the hole located at the Cu atom and the electron at the phenazine moiety this  $^3\text{MLCT}$  state shows no phosphorescence and can be considered as a dark state. Its lifetime is only 14.5 ns as it was determined by transient absorption spectroscopy on the nanosecond timescale using for excitation a YAG-laser system electronically synchronized to the white light probe. The  $^3\text{MLCT}$  lifetime is short compared to CuPS showing good performance such as **Cu1** and **Cu2** and probably responsible for the low activity of **Cu8** [73]. The same holds for **Cu7** and to some extent for **Cu6**.

Also various other copper complexes were studied by ultrafast pump-probe spectroscopy [77, 78]. They all show dynamics on the picosecond timescale which can be related to ISC and structural relaxation processes. Two further examples are given here. In case of heteroleptic complexes based on the structure  $[\text{Cu}(\text{I})(\text{Xantphos})(4H\text{-imidazolate})]$  subpicosecond ISC was observed, followed by the planarization of the *N*-aryl rings with respect to the *4H*-imidazolate plane, the latter process taking place on a 10 ps timescale [77]. The fast ISC rate was explained by strong spin-orbit coupling due to similar dihedral angles and geometries of the excited singlet and triplet state in this class of molecules. In a series of homoleptic complexes with phenanthroline based ligands light induced dynamics again on the subpicosecond and the 10 ps timescale were found [78]. The complex with the smallest capability for structural relaxation showed the fastest dynamics indicating that large structural distortions slow down the processes.

### 3.2. Iron complexes

In the quest for photosensitizers based on abundant metals iron complexes come more and more to the fore [27, 46]. They are well available and their absorption spectra are in the visible and can be efficiently tuned by the ligands making these complexes attractive candidates. However, they suffer from an extraordinary short lifetime of the photochemical active  $^3\text{MLCT}$  state which is often shorter than 100 fs [79–81]. The reason are low lying metal centered (MC) states which cause an efficient radiationless relaxation channel back to the electronic ground state, see figure 5. The  $^3\text{MLCT}$  state is quickly depopulated by the  $^3\text{MC}$  state which couples also to the potential energy surface of the ground state, see figure 5. In the isoelectronic ruthenium complexes this does not happen since their MC states are energetically above the MLCT states resulting in favorable  $^3\text{MLCT}$  lifetimes [46].

Different approaches to increase the MLCT lifetime are currently investigated. The goal is to destabilize the MC state applying ligands which, e.g., enforce a high symmetry or have a strong  $\pi$ - or  $\sigma$ -donating character [27]. In this context M. Bauer and coworkers studied the influence of strong  $\sigma$ -donation induced by *N*-heterocyclic carbene (NHC) ligands [61]. The number of the NHC ligands was systematically increased resulting in a progressive rise of the energy of the  $e_g$  orbitals and destabilization of the MC states. The structures of the complexes are shown in figure 6.

The impact of the NHC-ligands on the lifetime of the  $^3\text{MLCT}$  state was studied by ultrafast absorption spectroscopy [61]. Figure 7 shows exemplary transient absorption spectra obtained after optical excitation at 550 nm for complex **Fe3** containing three Fe-carbene groups. The transient absorption is dominated by ground state bleach and its recovery. At



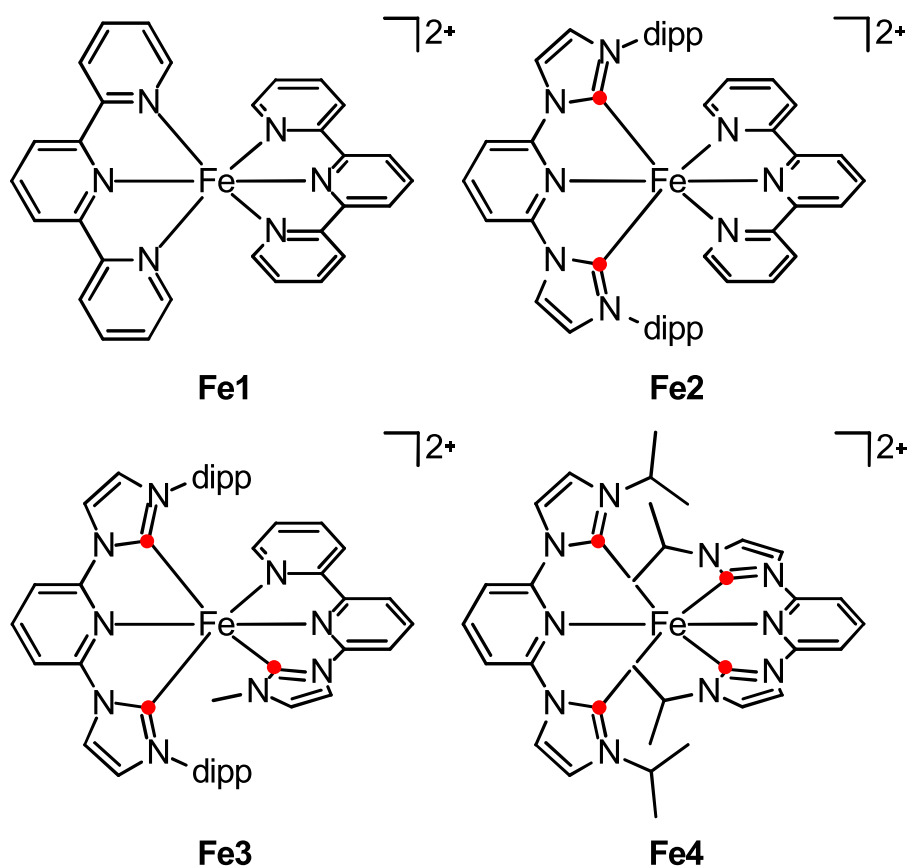


**Figure 6.** Iron complexes with NHC-ligands (with dipp = diisopropylphenyl) in comparison to the bis(terpyridine)iron(II) complex **Fe1**. The red dots mark the positions of the  $\sigma$ -donating carbene sites [61].

wavelengths above 620 nm an excited state absorption (ESA) is found which decays quickly. Since the reduced form of **Fe3** shows there also absorption the ESA can be regarded as a signature of an excess electron on the ligand and population of a charge transfer state. The dynamics can be fitted with a biexponential decay with time constants of 3.6 ps and 32 ps. The DAS of the 32 ps component resembles the inverse of the stationary absorption and reflects the return to the electronic ground state. The 3.6 ps component has a similar shape but contains the ESA band in the red indicating a charge transfer contribution. The findings point to the following scenario. ISC from the optically populated  $^1\text{MLCT}$  to the  $^3\text{MLCT}$  state is in iron complexes faster than the time resolution of transient absorption measurements with a WLC as probe. The 3.6 ps component reflects the depopulation of the  $^3\text{MLCT}$  state to the  $^3\text{MC}$  state which relaxes subsequently back to the electronic ground state within 32 ps. The  $^5\text{MC}$  state plays very probably no role. Otherwise a longer living component is expected since the decay of the  $^5\text{MC}$  state should be slow due to a necessary change of the spin quantum number by two.

In the case of fast intersystem crossing or internal conversion from the MLCT to a MC state electronic energy has to be efficiently converted to vibrational energy resulting in the excitation of vibrational modes and phonons. This occurs if either the energy gap between the two involved potential energy surfaces is small or strong vibronic coupling exists reflected by a pronounced relative shift of the surfaces along a nuclear coordinate. In the iron(II) complexes intersystem

crossing corresponds to the first case while the transition to the MC state is better described by the second case (see figure 5). In the latter situation some specific vibrational modes tuning the energy difference between the two surfaces are primarily excited and intramolecular vibrational redistribution (IVR) distributes in a second step the energy within several hundred femtoseconds also over the other modes. Signatures for IVR are often seen in ultrafast absorption measurements. They do not show up here because the rate of the internal conversion is slower than the IVR process. Furthermore, ESA and bleach bands are broad and changes of their shape due to IVR are then weak.

The time constants obtained for the other iron complexes are summarized in table 2 [61]. For none or two NHC groups the  $^3\text{MLCT}$  lifetime is in the order or below 100 fs and increases then to 3.6 ps and 8.1 ps for three and four NHC donor functions. This is a clear indication that with increasing  $\sigma$ -donation the  $^3\text{MLCT}$  lifetime lengthens and corresponding synthetic strategies are indeed successful. It is interesting to note that the  $^3\text{MC}$  lifetime shortens with increasing number of NHC moieties and destabilization of the MC state (see table 2). It indicates that with increasing MC energy a crossing of the ground state potential with the MC potential shifts towards the MC minimum and the energy barrier for the relaxation channel decreases accordingly, see figure 5.

Ultrafast absorption studies on iron complexes with other NHC-ligands are in line with the above findings and show that even longer lifetimes of the MLCT state are possible. By

adding electron withdrawing carboxyl groups to ligands with in total four NHC sites and extending the delocalization of the acceptor orbitals a successive increase of the MLCT lifetime from 9 ps to 26 ps was achieved [59, 83–86]. Using more strongly  $\sigma$ -donating mesoionic NHC ligands resulted in a lifetime of 13 ps [87] and increasing their total number of NHC sites to six in a record lifetime of 528 ps [56].

Also other strategies are applied for shaping the electronic structure of iron(II) complexes and their success is typically assessed by ultrafast absorption spectroscopy [27]. Enforcing a nearly perfect octahedral symmetry leads in  $[\text{Fe}(\text{dcp})_2]^{2+}$  ( $\text{dcp}$  = 2,6-bis(2-carboxypyridyl)pyridine) together with the low lying  $\pi^*$ -orbitals of the ligands to a strong destabilization of particularly the  $^5\text{MC}$  state. The observed lifetime of 0.28 ns is tentatively attributed to the  $^3\text{MC}$  state which probably is located below the  $^5\text{MC}$  state contrary to other iron complexes such as  $[\text{Fe}(\text{bpy})_3]^{2+}$  ( $\text{bpy}$  = 2,2'-bipyridine) [53]. In case of the heteroleptic complex  $[\text{Fe}(\text{dcp})(\text{ddpd})]^{2+}$  ( $\text{ddpd}$  = *N,N'*-dimethyl-*N,N'*-dipyridine-2-yl-pyridine-2,6-diamine) this approach is combined with a push-pull ligand set to lower the energy of the MLCT states while the energetic rise of the MC states is conserved. This results in a slower ground state recovery after optical excitation with a time constant of 0.55 ns which is again assigned to the lifetime of the  $^3\text{MC}$  state [54]. Cyclometalating ligands can be used to stabilize the MLCT states due to their strongly  $\pi$ -donating character while they have less influence on the energy of the MC states [55, 62, 63]. In the case of  $[\text{Fe}(\text{pbpy})(\text{tpy})]^+$  ( $\text{Hpbpy}$  = 6-phenyl-2,2'-bipyridine,  $\text{tpy}$  = 2,2':6',2''-terpyridine) the cyclometalating ligand pbpy leads to a red shifted absorption spectrum due to the decreased MLCT energy and a lifetime of this state of 0.8 ps which is 5.5 times larger than in the related complex  $[\text{Fe}(\text{tpy})_2]^{2+}$  [88]. Another approach is to design complexes with a high-spin ground state. This can be achieved by ligands causing steric strain such as dichloro- and dibromotpy [57, 58]. In the reported examples the  $^5\text{MC}$  state has a similar energy as the  $^1\text{A}$  ground state and is partially occupied at room temperature. Optical excitation results then in population of the  $^5\text{MLCT}$  or  $^7\text{MLCT}$  state which exhibit lifetimes of up to 17.4 ps. The dipole allowed transition from the  $^5\text{MC}$  to the  $^5\text{MLCT}$  causes an additional contribution to the stationary absorption spectrum which is underneath the band resulting from the transition from the  $^1\text{A}$  to the  $^1\text{MLCT}$  state [57].

In summary, the achieved lifetimes of the MLCT states are already promising for heterogeneous photocatalytic systems since electron injection into the conduction band of a semiconductor is usually very fast provided that the band edge is below the energy of the donating ligand orbital. In the context of dye sensitized solar cells light induced charge injection from iron(II) complexes into semiconductors such as  $\text{TiO}_2$  is already reported for several cases [84, 86]. For application in homogeneous systems the lifetime has to be further increased by about two to three orders of magnitude. Combining different strategies is a promising approach to achieve this challenging goal. Recently, new iron(III) complexes were reported which show luminescence from a ligand-to-metal charge transfer (LMCT) state [89, 90]. In these compounds both, the ground and the optically accessible LMCT state are duplets. It was possible to

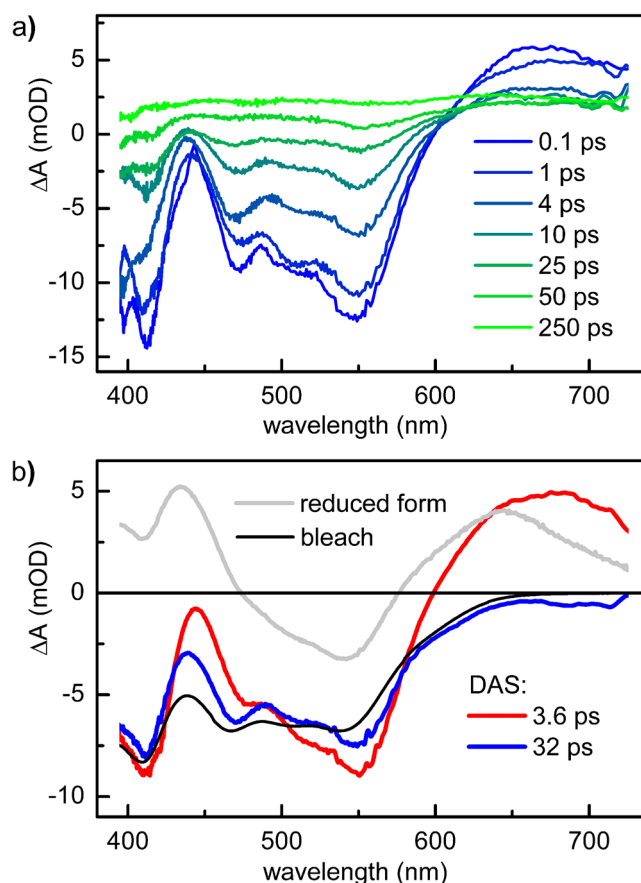


**Figure 7.** (a) Transient absorption spectra for the given delay times after optical excitation of **Fe3** at 550 nm. (b) DAS of the 3.6 ps (red line) and 32 ps (blue line) component obtained by a biexponential fit to the data. The inverted steady-state absorption (black line, bleach) and the difference spectrum for the reduced complex (grey line) are shown for comparison, adapted from [61]. Copyright © 2018, American Chemical Society.

**Table 2.** Lifetimes of the MLCT and MC states of the iron complexes **Fe1–Fe4** [61].

Compound	$\tau_{\text{MLCT}}$ (ps)	$\tau_{\text{MC}}$ (ps)
<b>Fe1</b>	0.145 <sup>a</sup>	4000–5000 <sup>a,b</sup>
<b>Fe2</b>	<0.1	173
<b>Fe3</b>	3.6	32
<b>Fe4</b>	8.1	$\ll 8$

<sup>a</sup> Liu *et al* [59].

<sup>b</sup> McCusker *et al* [82].

stabilize by ligand design the LMCT state sufficiently strong to obtain a lifetime even in the nanosecond regime and thereby photoluminescence. The onset of the ground state absorption of these complexes is strongly blue shifted with respect to the corresponding iron(II) complexes. Nevertheless, they are very promising candidates for future applications.

#### 4. Time-resolved photoluminescence and quenching experiments

For a photocatalytic system the interaction of the photosensitizer with the other components of the system is a key

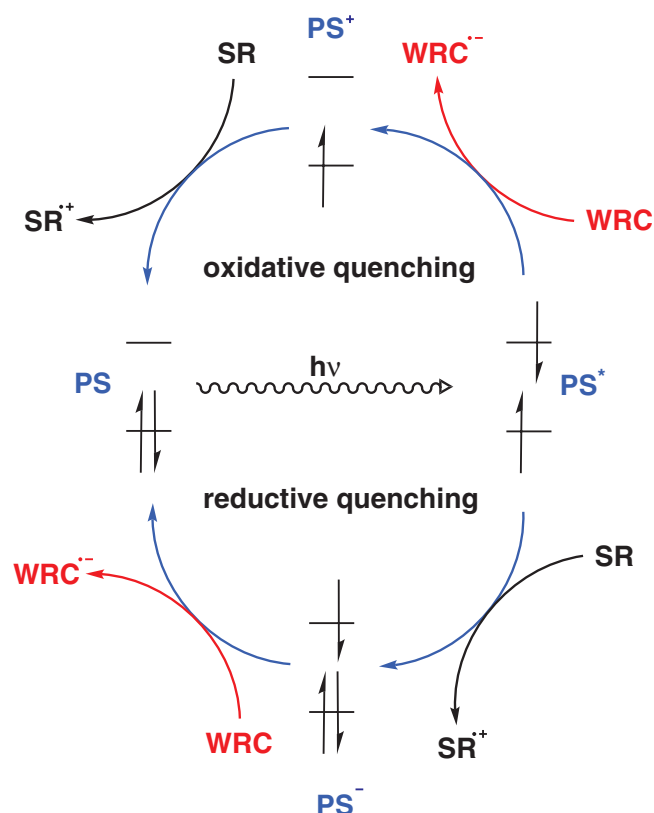


**Figure 8.** Oxidative and reductive quenching path for a photosensitizer (PS) interacting with a sacrificial reductant (SR) and a water reduction catalyst (WRC) [52, 91].

element. In the case of a water reducing half reaction, as it is exemplary discussed in this review, the goal is to achieve after optical excitation efficient electron transfer from an electron donating substrate to the sensitizer as well as from the sensitizer to the catalyst, see figure 1. Since the first electron transfer steps lead to a depopulation of an electronically excited state, in the here discussed cases a  $^3MLCT$  state, the lifetime of this state is reduced and its emission quenched [42]. Time-resolved luminescence experiments provide a powerful tool to characterize the quenching efficiency and the interaction probability of the photosensitizer with other components of system by measuring the reduction of the lifetime in the presence of potential reaction partners.

Two scenarios are possible which differ in the sequence of the electron transfer steps, see figure 8 [52, 91]. In the case of oxidative quenching first an electron is transferred from the excited photosensitizer to the catalyst changing the sensitizer to its oxidized form. The original sensitizer is restored in a second step by an electron transfer from an electron donating substrate. In reductive quenching these two steps are interchanged and the reduced sensitizer is formed as intermediate. Comparing the reduction of the  $^3MLCT$  lifetime of the photosensitizer in the presence of one or the other of the electron transfer partners allows to discriminate both pathways [24, 52].

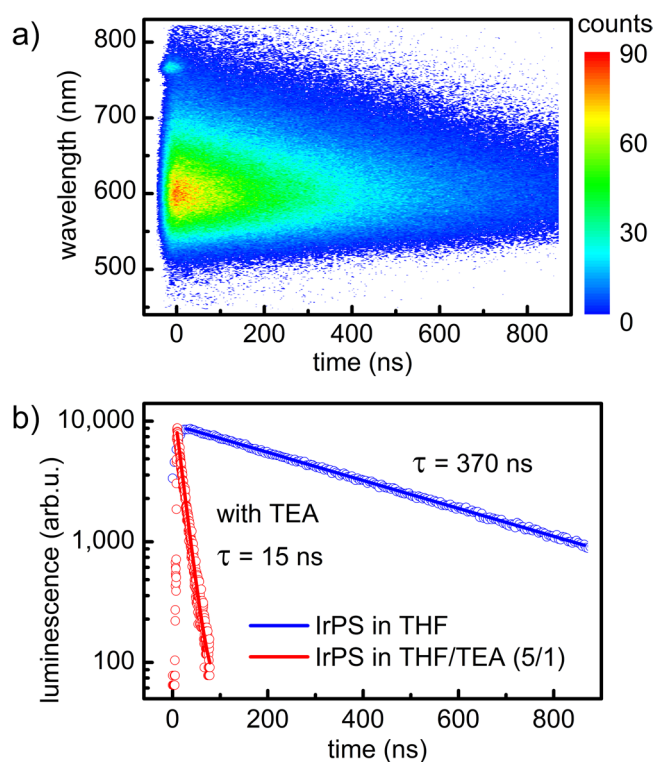


**Figure 9.** (a) Time dependent luminescence spectrum of **Ir1** in THF. (b) Luminescence kinetics and lifetimes of **Ir1** in THF without (blue) and with trimethylamine (TEA, red). (b) Reproduced from [24]. CC BY 4.0.

#### 4.1. Iridium photosensitizers and reductive quenching

Iridium complexes are applied as photosensitizers in photocatalytic hydrogen generation since they result in excellent photon-to-hydrogen yields of up to 48% [24]. Beller and coworkers considered in detail a homogeneous system containing the iridium complex  $[Ir(ppy)_2(bpy)]PF_6$  (**Ir1**,  $ppy$  = monodeprotonated 2-phenylpyridine,  $bpy$  = 2,2'-bipyridine) as photosensitizer, TEA as sacrificial reductant, and  $[HFe_3(CO)_{11}][NEt_3H]$  as water reduction catalyst [22].

Time-resolved luminescence studies applying a streak camera system were performed to investigate the interaction of **Ir1** with TEA and the catalyst (see figure 9) [22]. For **Ir1** in oxygen-free tetrahydrofuran (THF) the  $^3MLCT$  lifetime was determined to 370 ns. Adding the catalyst with a concentration of  $1.6 \times 10^{-5}$  M to the solution resulted in a lifetime of 280 ns while in a solution containing TEA with a volume ratio of THF:TEA 5:1, which was also used in the photocatalytic experiments, the lifetime was drastically quenched to 15 ns [24]. This shows that in this photocatalytic system the electron transfer sequence evolves along the reductive pathway.

From a series of measurements with different concentrations of TEA a bimolecular quenching rate of  $k_q = 5.9 \cdot 10^7 \text{ M}^{-1} \text{ s}^{-1}$  was determined. This result has to be compared to the diffusion controlled bimolecular collision rate  $k_{coll}$  which can be calculated by means of the Stokes-Einstein formula making use of equation (1) [39]:

$$k_{\text{coll}} = \frac{4\pi}{1000} N_A \cdot (R_{\text{donor}} + R_{\text{acceptor}}) \cdot D$$

$$\text{with } D = \frac{k_B T}{6\pi\eta} \left( \frac{1}{R_{\text{donor}}} + \frac{1}{R_{\text{acceptor}}} \right). \quad (1)$$

The mutual diffusion coefficient  $D$  of the electron donor and acceptor, i.e. in the present case of TEA and **Ir1**, depends on the temperature  $T$ , the viscosity  $\eta$  of the solvent, and the gyration radii  $R_{\text{donor}}$  and  $R_{\text{acceptor}}$  of the donor and acceptor, respectively.  $N_A$  is the Avogadro number and  $k_B$  the Boltzmann constant and the distance of closest approach is estimated as sum of the gyration radii. The latter were obtained from molecular geometries determined by DFT calculations [22]. The structures were optimized without symmetry restrictions applying the optimally-tuned LC-BLYP functional combined with the LANL2DZ ECP basis set for iridium and the 6-31G(d) basis set for all other atoms. Effects due to the solvent were included via the polarizable continuum model. The gyration radius is finally evaluated from the positions of the atoms with respect to the center of mass of the molecule.

The radii of TEA and **Ir1** were determined to 2.5 Å and 4.2 Å, respectively, and a collision rate of  $k_{\text{coll}} = 1.4 \cdot 10^{10} \text{ M}^{-1} \text{ s}^{-1}$  was obtained from equation (1). Comparing this value to the quenching rate shows that only one out of about 200 collisions results in a quenching event [22]. DFT calculations were applied to understand this finding. They showed that only at specific collision geometries electron transfer from TEA to **Ir1** is energetically favored and quenching possible. Most collisions occur with unsuitable orientations of the reaction partners and do not deactivate the  $^3\text{MLCT}$  state of the iridium complex. Interestingly, the quenching rate  $k_q = 6.6 \cdot 10^{10} \text{ M}^{-1} \text{ s}^{-1}$  of the iron catalyst, again determined by time-resolved luminescence measurements, is much closer to the corresponding bimolecular collision rate  $k_{\text{coll}} = 1.5 \cdot 10^{11} \text{ M}^{-1} \text{ s}^{-1}$  indicating that in this case quenching is nearly diffusion limited [22]. Here the collision rate is calculated by the Debye relation applying equation (2) [92]:

$$k_{\text{coll}} = \frac{8N_A k_B T \cdot b}{3000\eta(e^b - 1)} \quad \text{and} \quad b = \frac{Z_{\text{donor}} Z_{\text{acceptor}} e_0^2}{4\pi(R_{\text{donor}} + R_{\text{acceptor}})\varepsilon_r \varepsilon_0 k_B T} \quad (2)$$

$e_0$  denotes the elementary charge,  $\varepsilon_0$  the vacuum permittivity, and  $\varepsilon_r$  the dielectric constant of the solvent. The collision rate depends on the gyration radii  $R_{\text{donor}}$  and  $R_{\text{acceptor}}$  of the electron donor and acceptor, i.e. the reduced **Ir1** and the iron catalyst, as well as on their charge numbers  $Z_{\text{donor}}$  and  $Z_{\text{acceptor}}$ , here +1 and -1. With the radii 4.2 Å and 3.0 Å for **Ir1** and the catalyst, respectively, the above given collision rate was obtained.

Even though quenching by the iron catalyst is more efficient, quenching by TEA is much faster and the by far dominant process due to the considerable volume fraction and high concentration of TEA in the photocatalytic system. This allows for a high total transfer yield along the reductive path and is a prerequisite for the high efficiency of the system [22]. It should also be mentioned that an analysis of the redox potentials indicates that in the case of the iron catalyst

quenching is probably caused by energy transfer and not by an electron transfer process.

Furthermore, it would be desirable to determine experimentally the diffusion constants of the involved compounds in order to support the performed analysis. This is e.g. possible by dedicated experiments based on nuclear magnetic resonance spectroscopy [93].

## 4.2. Copper photosensitizers and oxidative quenching

In the case of copper photosensitizers, the situation is different as time-resolved luminescence studies on the complex **Cu1** (see figure 3) show [24]. It is applied in a homogeneous photocatalytic system very similar to the one facilitating the iridium photosensitizer. The same iron complex is used as water reduction catalyst and TEA as sacrificial electron donor [24, 94]. In pure THF a lifetime of the  $^3\text{MLCT}$  state of 2.9  $\mu\text{s}$  was found for a **Cu1** concentration of 0.35 mM which is applied in the photocatalytic system. Adding 17 vol % of TEA causes a moderate reduction of the luminescence lifetime to 1  $\mu\text{s}$ , while it is strongly reduced down to 50 ns if the solution also contains 0.5 mM of the catalyst [24]. This demonstrates that the oxidative path prevails and the excited **Cu1** delivers an electron to the catalyst before it accepts an electron from a TEA molecule.

Using acetonitrile (ACN) as solvent, time-resolved emission measurements reveal the same general picture [23]. However, in ACN intramolecular relaxation in **Cu1** is faster and the  $^3\text{MLCT}$  lifetime is only 280 ns. TEA has only a small impact on the lifetime and quenches it to 210 ns while adding 0.5 mM of the iron catalyst reduces the lifetime to only 100 ns corresponding to a bimolecular quenching rate of  $k_{\text{bi}} = 1.2 \cdot 10^{10} \text{ M}^{-1} \text{ s}^{-1}$  [23].

The presented examples demonstrate that time-resolved photoluminescence is a powerful approach to discriminate between reductive and oxidative pathways and to characterize the interaction of the photosensitizer with the other components of a photocatalytic system.

## 5. Electron transfer yield from transient absorption measurements

While photoluminescence experiments are very sensitive and versatile in characterizing quenching processes, they are only monitoring the excited state population and provide little information about the outcome of these processes. Pump-probe absorption spectroscopy extending to longer timescales, traditionally called flash photolysis, can solve this problem. In the transient spectra repopulation of the original ground state shows up as recovery of the bleach signal while electron transfer results in new spectral features associated with the oxidized and reduced forms of the electron donor and acceptor, respectively. If the extinction coefficient of one of these two species is known one can even quantitatively evaluate the electron transfer yield. In understanding the behavior of photocatalytic systems this is highly valuable since one can assess



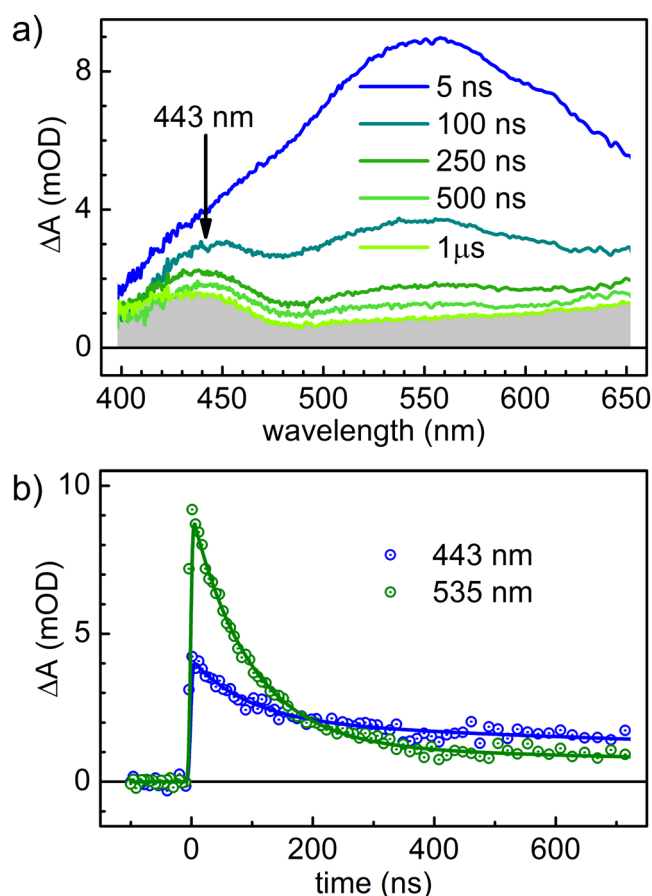


**Figure 10.** (a) Transient absorption spectra after optical excitation of **CuI** in acetonitrile in the presence of the iron catalyst. (b) Corresponding time traces at the probe wavelengths 443 nm and 535 nm. Adapted from [23].

if quenching of the photosensitizer comes with losses which limit the performance of the system.

In the following the approach is discussed by means of transient absorption studies on the electron transfer from the copper sensitizer **CuI** to the iron based water reduction catalyst  $[\text{HFe}_3(\text{CO})_{11}]^-$  [23]. As already mentioned, this is the first transfer step of the photocatalytic system introduced above, see figure 1. The experimental setup providing a time resolution of 7 ns is sketched in section 2. As solvent acetonitrile was used since it allows for higher concentrations of **CuI** which is advantageous for the transient absorption signals. After optical excitation the pump-probe spectra exhibit the same excited state absorption as the femtosecond measurements on the sub-ns timescale. Without catalyst this absorption decays completely with a time constant of 280 ns which is as expected identical to the lifetime of the  $^3\text{MLCT}$  state of **CuI** in acetonitrile obtained via photoluminescence, see above. No transient absorption change remains demonstrating that all optically excited complexes return back to the ground state. In the presence of  $5 \cdot 10^{-4}$  M of the iron catalyst the decay of the excited state absorption accelerates to 100 ns, again in agreement with time-resolved emission measurements, and a long-living absorption signal is found exhibiting a characteristic band at 443 nm, see figure 10 [23].

To identify the origin of this band control experiments with methyl viologen  $[\text{MV}][\text{Cl}_2]$  as electron acceptor instead of the catalyst were performed. While the original dication  $\text{MV}^{2+}$  does not absorb in the visible the electron transfer product  $\text{MV}^{1+}$  exhibits there two characteristic bands [29]. In the control measurements they appear together with a band at 443 nm demonstrating that electron transfer occurs and the band at 443 nm results from the oxidized copper sensitizer. From the strength of the absorption bands belonging to  $\text{MV}^{1+}$  the concentration of this species was determined [23]. The concentration of the oxidized sensitizer has to be same since both species are formed by the electron transfer processes. Making use of this fact the extinction coefficient  $\varepsilon = 2360 (\text{M cm})^{-1}$  of the oxidized copper complex at 443 nm was obtained. It was then employed to determine the concentration of the electron transfer products in the photocatalytic system. It turned out that only about 30% of the collisions between optically excited **CuI** and catalyst leading to quenching result indeed in electron transfer. The other quenching events just deactivate the copper complex and represent a high loss [23]. Future design strategies have also to care about this loss channel.

In summary, transient absorption measurements on longer time scales are not only suitable to identify electron transfer products and to prove that the process takes indeed place but also provide quantitative information about its efficiency and yield as well as the contribution of non-reactive loss channels.

## 6. Summary and conclusions

By means of selected examples it is shown that time-resolved spectroscopy is a powerful approach to obtain insights into the electronic dynamics of homogeneous photocatalytic systems and to understand reaction mechanisms and efficiency limiting factors. Several different techniques have to be combined in order to cover a wide range of timescales. Femtosecond pump-probe spectroscopy is the method of choice to study ultrafast intramolecular processes of the photosensitizers. Beside of many other applications it was successfully applied to characterize geometric relaxation processes and intersystem crossing in copper complexes as well as the population of a dark state in such a complex with an extended  $\pi$ -system. It is also highly valuable in investigating iron complexes, which suffer from a fast intramolecular relaxation channel via a metal centered state, and in assessing design strategies for slowing down this channel. Population and lifetime of electronically excited states such as the in many metal complexes photocatalytically active  $^3\text{MLCT}$  state can be efficiently characterized by time-resolved emission spectroscopy. Applying a streak camera provides spectral resolution and at the same time access to timescales from picoseconds to many microseconds. The analysis of photoluminescence quenching reveals insights into the interaction between molecular components resulting e. g. in bimolecular reactions and intermolecular charge transfer. For a hydrogen generating system utilizing an iridium sensitizer it is found by such experiments in combination with theoretical calculations that the electron transfer from a donor substrate

to the metal complex calls for specific collision geometries and is therefore rather improbable. However, the long triplet lifetime of the iridium complex in combination with a high substrate concentration leads nevertheless to an efficient system following a reductive pathway. In the case of heteroleptic copper sensitizers the corresponding system takes an oxidative path as shown again by time-resolved photoluminescence. To observe the products and to determine the yield of intramolecular electron transfer processes transient absorption measurements on timescales beyond single nanoseconds are suitable. The combination of a femtosecond white light probe with an electronically delayed YAG-laser system for excitation is a versatile and sensitive approach for corresponding pump-probe experiments. Transient absorption measurements on the copper based photocatalytic system not only demonstrate that electron transfer to the catalyst occurs but provide also absolute yields and information about the strength of non-reactive loss channels. In summary, combining the results of the various time-resolved spectroscopic techniques leads to a detailed picture of the behavior of the respective photosensitizer and of the first electron transfer steps in a photocatalytic system. The findings are highly valuable in the quest for improved systems and help to develop and assess new design strategies.

## 7. Outlook

In the coming years the intensive development, in particular, of copper and iron complexes will go one in order to obtain efficient and versatile photosensitizers. This work will be more and more routinely accompanied by time-resolved spectroscopic investigations to assess the performance of the compounds and guide their design. The interpretation of the spectroscopic results are already now heavily supported by *ab initio* calculations [22, 24, 54, 61, 87]. While they do a good job in determining the energies and equilibrium structures of electronic states and thus in modeling of spectral bands it is still difficult to obtain with sufficient accuracy the rates of electronic relaxation processes. However, using time-resolved experiments for direct comparison leads to rapid improvements and it is expected that at some point not too far in the future *ab initio* calculations will be able to predict the structures of functioning photosensitizers.

Another goal for the pump-probe techniques is to go beyond the electron transfer steps and to look also into the chemical processes at the catalyst and to establish a better overlap with other *in situ* and operando methods. In this way a fairly complete picture of the processes and mechanisms at work in a homogenous photocatalytic system should be feasible. The approach using a femtosecond whitelight continuum for probing and a YAG laser system for excitation can be more or less directly applied to time scales beyond a millisecond. However, two major challenges have to be addressed. One is that many interesting intermediates are only in very low concentrations present and the sensitivity of the discussed detection scheme has to be improved. The other is, that it is difficult to conclude from the optical signatures on the exact molecular structure of intermediates if no additional information is available. Here,

the combination with methods which are more sensitive to the structure such as infrared spectroscopy is a good strategy [14]. Several groups apply also infrared probing in pump-probe experiments which is in the context of photocatalysis a very powerful approach too and will be more intensively used in the future [95]. However, sensitivity is here as well an issue.

## Acknowledgment

We are very grateful to our former coworkers Antje Neubauer and Stefanie Tschierlei for their paramount contributions to our research. We thank Oliver Kühn, Katja Heinze, Matthias Bauer, and their groups as well as Henrik Junge, Matthias Beller, Angelika Brückner, and their coworkers from the Leibniz Institute for Catalysis for long-standing and very fruitful collaborations which are the basis of our work. Financial support by the Deutsche Forschungsgemeinschaft via the Priority Program SPP 2102 ‘Light-controlled reactivity of metal complexes’ (LO 714/11-1) and the Federal Ministry of Education and Research of Germany via the collaborative project ‘Light to Hydrogen’ (L2H), which was part of the program ‘Spitzenforschung und Innovation in den Neuen Ländern’, and the growth core ‘MikroLas—Surfaces shaped by photonics’ is gratefully acknowledged.

## ORCID iDs

Stefan Lochbrunner  <https://orcid.org/0000-0001-9729-8277>

## References

- [1] Armaroli N and Balzani V 2007 The future of energy supply: Challenges and opportunities *Angew. Chem., Int. Ed. Engl.* **46** 52–66
- [2] Schiermeier Q, Tollefson J, Scully T, Witze A and Morton O 2008 Electricity without carbon *Nature* **454** 816–23
- [3] Jacobson M Z 2009 Review of solutions to global warming, air pollution, and energy security *Energy Environ. Sci.* **2** 148–73
- [4] Arakawa H *et al* 2001 Catalysis research of relevance to carbon management: progress, challenges, and opportunities *Chem. Rev.* **101** 953–96
- [5] Lewis N S and Nocera D G 2006 Powering the planet: Chemical challenges in solar energy utilization *Proc. Natl Acad. Sci. USA* **103** 15729–35
- [6] Centi G and Perathoner S 2010 Towards solar fuels from water and CO<sub>2</sub> *ChemSusChem* **3** 195–208
- [7] Turner J A 2004 Sustainable hydrogen production *Science* **305** 972–4
- [8] Lubitz W and Tumas W 2007 Hydrogen: an overview *Chem. Rev.* **107** 3900–3
- [9] Roduner E 2014 Understanding catalysis *Chem. Soc. Rev.* **43** 8226–39
- [10] Schlögl R 2015 Heterogeneous catalysis *Angew. Chem., Int. Ed. Engl.* **54** 3465–520
- [11] Li X, Yu J, Low J, Fang Y, Xiao J and Chen X 2015 Engineering heterogeneous semiconductors for solar water splitting *J. Mater. Chem. A* **3** 2485–534
- [12] Esswein A J and Nocera D G 2007 Hydrogen production by molecular photocatalysis *Chem. Rev.* **107** 4022–47

- [13] Eckenhoff W T, McNamara W R, Du P and Eisenberg R 2013 Cobalt complexes as artificial hydrogenases for the reductive side of water splitting *Biochim. Biophys. Acta* **1827** 958–73
- [14] Gärtner F, Boddien A, Barsch E, Fumino K, Losse S, Junge H, Hollmann D, Brückner A, Ludwig R and Beller M 2011 Photocatalytic hydrogen generation from water with iron carbonyl phosphine complexes: Improved water reduction catalysts and mechanistic insights *Chem. Eur. J.* **17** 6425–36
- [15] Lubitz W, Reijerse E J and Messinger J 2008 Solar water-splitting into H<sub>2</sub> and O<sub>2</sub>: Design principles of photosystem II and hydrogenases *Energy Environ. Sci.* **1** 15–31
- [16] You Y and Nam W 2012 Photofunctional triplet excited states of cyclometalated Ir(III) complexes: Beyond electroluminescence *Chem. Soc. Rev.* **41** 7061–84
- [17] Riedle E and Wenninger M 2013 Time resolved spectroscopy in photocatalysis *Chemical Photocatalysis* ed B König (Berlin: de Gruyter & Co) pp 319–86
- [18] Arias-Rotondo D M and McCusker J K 2016 The photophysics of photoredox catalysis: a roadmap for catalyst design *Chem. Soc. Rev.* **45** 5803–20
- [19] Carey M C, Adelman S L and McCusker J K 2019 Insights into the excited state dynamics of Fe(II) polypyridyl complexes from variable-temperature ultrafast spectroscopy *Chem. Sci.* **10** 134–44
- [20] Hammarström L, Lomoth R, Ponseca C S, Chabera P, Uhlig J and Sundström V 2018 Time-resolved laser spectroscopy in molecular devices for solar energy conversion *Molecular Devices for Solar Energy Conversion and Storage* ed H Tian *et al* (Singapore: Springer) pp 385–432
- [21] Schroot R, Schlotthauer T, Dietzek B, Jäger M and Schubert U S 2017 Extending long-lived charge separation between donor and acceptor blocks in novel copolymer architectures featuring a sensitizer core *Chem. Eur. J.* **23** 16484–90
- [22] Neubauer A *et al* 2014 Electron- and energy-transfer processes in a photocatalytic system based on an Ir(III)-photosensitizer and an iron catalyst *J. Phys. Chem. Lett.* **5** 1355–60
- [23] Friedrich A, Bokareva O S, Luo S P, Junge H, Beller M, Kühn O and Lochbrunner S 2018 Effective quenching and excited-state relaxation of a Cu(I) photosensitizer addressed by time-resolved spectroscopy and TDDFT calculations *Chem. Phys.* **515** 557–63
- [24] Junge H, Rockstroh N, Fischer S, Brückner A, Ludwig R, Lochbrunner S, Kühn O and Beller M 2017 Light to hydrogen: photocatalytic hydrogen generation from water with molecularly-defined iron complexes *Inorganics* **5** 14
- [25] McCullough B J, Neyhouse B J, Schrage B R, Reed D T, Osinski A J, Ziegler C J and White T A 2018 Visible-light-driven photosystems using heteroleptic Cu(I) photosensitizers and Rh(III) catalysts to produce H<sub>2</sub> *Inorg. Chem.* **57** 2865–75
- [26] Saeedi S, Xue C, McCullough B J, Roe S E, Neyhouse B J and White T A 2019 Probing the diphosphine ligand's impact within heteroleptic, visible-light-absorbing Cu(I) photosensitizers for solar fuels production *ACS Appl. Energy Mater.* **2** 131–43
- [27] Wenger O S 2019 Is iron the new ruthenium? *Chem. Eur. J.* **25** 6043–52
- [28] Giereth R, Frey W, Junge H, Tschierlei S and Karnahl M 2017 Copper photosensitizers containing P<sup>^</sup>N ligands and their influence on photoactivity and stability *Chem. Eur. J.* **23** 17432–7
- [29] Lomoth R, Häupl T, Johansson O and Hammarström L 2002 Redox-switchable direction of photoinduced electron transfer in an Ru (bpy)<sub>3</sub><sup>2+</sup>-viologen dyad *Chem. Eur. J.* **8** 102–10
- [30] Brückner A 2010 *In situ* electron paramagnetic resonance: a unique tool for analyzing structure-reactivity relationships in heterogeneous catalysis *Chem. Soc. Rev.* **39** 4673–84
- [31] Goetzl S, Teutloff C, Werther T, Hennig S E, Jeoung J H, Bittl R and Dobbek H 2017 Protein dynamics in the reductive activation of a B12-containing enzyme *Biochemistry* **56** 5496–502
- [32] Balzani V, Moggi L, Manfrin M F, Bolletta F and Laurence G S 1975 Quenching and sensitization processes of coordination compounds *Coord. Chem. Rev.* **15** 321–433
- [33] Engleitner S, Seel M and Zinth W 1999 Nonexponentialities in the ultrafast electron-transfer dynamics in the system oxazine 1 in *N,N*-dimethylaniline *J. Phys. Chem. A* **103** 3013–9
- [34] Ernsting N P and Kaschke M 1991 A reliable pump-probe, broadband spectrometer for subpicosecond transient absorption *Rev. Sci. Instrum.* **62** 600–8
- [35] Krebs N, Pugliesi I and Riedle E 2013 Pulse compression of ultrashort UV pulses by self-phase modulation in bulk material *Appl. Sci.* **3** 153–67
- [36] Riedle E, Beutler M, Lochbrunner S, Piel J, Schenkl S, Spörlein S and Zinth W 2000 Generation of 10–50 fs pulses tunable through all of the visible and the NIR *Appl. Phys. B* **71** 457–65
- [37] Cerullo G and De Silvestri S 2003 Ultrafast optical parametric amplifiers *Rev. Sci. Instrum.* **74** 1–18
- [38] Lessing H E and von Jena A 1976 Separation of rotational diffusion and level kinetics in transient absorption spectroscopy *Chem. Phys. Lett.* **42** 213–7
- [39] Valeur B 2002 *Molecular Fluorescence* (Weinheim: Wiley)
- [40] Lakowicz J R 2006 *Principles of Fluorescence Spectroscopy* (New York: Springer)
- [41] O'Connor D V and Phillips D 1984 *Time-Correlated Single Photon Counting* (London: Academic)
- [42] Juris A and Balzani V 1988 Ru(II) polypyridine complexes: photophysics, photochemistry, electrochemistry, and chemiluminescence *Coord. Chem. Rev.* **84** 85–277
- [43] Lowry M S and Bernhard S 2006 Synthetically tailored excited states: phosphorescent, cyclometalated iridium(III) complexes and their applications *Chem. Eur. J.* **12** 7970–7
- [44] Zhang Y, Schulz M, Wächter M, Karnahl M and Dietzek B 2018 Heteroleptic diimine–diphosphine Cu(I) complexes as an alternative towards noble-metal based photosensitizers: design strategies, photophysical properties and perspective applications *Coord. Chem. Rev.* **356** 127–46
- [45] Iwamura M, Takeuchi S and Tahara T 2015 Ultrafast excited-state dynamics of copper(I) complexes *Acc. Chem. Res.* **48** 782–91
- [46] McCusker J K 2019 Electronic structure in the transition metal block and its implications for light harvesting *Science* **363** 484–8
- [47] Hashimoto M, Igawa S, Yashima M, Kawata I, Hoshino M and Osawa M 2011 Highly efficient green organic light-emitting diodes containing luminescent three-coordinate copper(I) complexes *J. Am. Chem. Soc.* **133** 10348–51
- [48] Zhang Q, Komino T, Huang S, Matsunami S, Goushi K and Adachi C 2012 Triplet exciton confinement in green organic light-emitting diodes containing luminescent charge-transfer Cu(I) complexes *Adv. Funct. Mater.* **22** 2327–36
- [49] Liu Z, Qayyum M F, Wu C, Whited M T, Djurovich P I, Hodgson K O, Hedman B, Solomon E I and Thompson M E 2011 A codeposition route to CuI-pyridine coordination complexes for organic light-emitting diodes *J. Am. Chem. Soc.* **133** 3700–3
- [50] Yersin H, Rausch A F, Czerwieniec R, Hofbeck T and Fischer T 2011 The triplet state of organo-transition metal compounds. Triplet harvesting and singlet harvesting for efficient OLEDs *Coord. Chem. Rev.* **255** 2622–52



- [51] Bizzarri C, Spuling E, Knoll D M, Volz D and Bräse S 2018 Sustainable metal complexes for organic light-emitting diodes (OLEDs) *Coord. Chem. Rev.* **373** 49–82
- [52] Luo S P *et al* 2013 Photocatalytic water reduction with copper-based photosensitizers: a noble-metal-free system *Angew. Chem., Int. Ed. Engl.* **52** 419–23
- [53] Jamula L L, Brown A M, Guo D and McCusker J K 2014 Synthesis and characterization of a high-symmetry ferrous polypyridyl complex: approaching the  $^5T_2/{}^3T_1$  crossing point for Fe<sup>II</sup> *Inorg. Chem.* **53** 15–7
- [54] Mengel A K C, Förster C, Breivogel A, Mack K, Ochsmann J R, Laquai F, Ksenofontov V and Heinze K 2015 A heteroleptic push-pull substituted iron(II) bis(tridentate) complex with low-energy charge-transfer states *Chem. Eur. J.* **21** 704–14
- [55] Mukherjee S, Bowman D N and Jakubikova E 2015 Cyclometalated Fe(II) complexes as sensitizers in dye-sensitized solar cells *Inorg. Chem.* **54** 560–9
- [56] Chábera P *et al* 2018 Fe<sup>II</sup> hexa *N*-heterocyclic carbene complex with a 528 ps metal-to-ligand charge-transfer excited-state lifetime *J. Phys. Chem. Lett.* **9** 459–63
- [57] Fatur S M, Shepard S G, Higgins R F, Shores M P and Damrauer N H 2017 A synthetically tunable system to control MLCT excited-state lifetimes and spin states in iron(II) polypyridines *J. Am. Chem. Soc.* **139** 4493–505
- [58] Shepard S G, Fatur S M, Rappé A K and Damrauer N H 2016 Highly strained iron(II) polypyridines: exploiting the quintet manifold to extend the lifetime of MLCT excited states *J. Am. Chem. Soc.* **138** 2949–52
- [59] Liu Y *et al* 2013 Towards longer-lived metal-to-ligand charge transfer states of iron(II) complexes: an *N*-heterocyclic carbene approach *Chem. Commun.* **49** 6412–4
- [60] Leshchev D *et al* 2018 Tracking the picosecond deactivation dynamics of a photoexcited iron carbene complex by time-resolved x-ray scattering *Chem. Sci.* **9** 405–14
- [61] Zimmer P *et al* 2018 The connection between NHC ligand count and photophysical properties in Fe(II) photosensitizers: An experimental study *Inorg. Chem.* **57** 360–73
- [62] Dixon I M, Khan S, Alary F, Boggio-Pasqua M and Heully J L 2014 Probing the photophysical capability of mono and bis(cyclometallated) Fe(II) polypyridine complexes using inexpensive ground state DFT *Dalton Trans.* **43** 15898–905
- [63] Dixon I M, Alary F, Boggio-Pasqua M and Heully J L 2015 Reversing the relative  ${}^3\text{MLCT}$ - ${}^3\text{MC}$  order in Fe(II) complexes using cyclometallating ligands: a computational study aiming at luminescent Fe(II) complexes *Dalton Trans.* **44** 13498–503
- [64] Armaroli N 2001 Photoactive mono- and polynuclear Cu(I)-phenanthrolines. A viable alternative to Ru(II)-polypyridines? *Chem. Soc. Rev.* **30** 113–24
- [65] Sandroni M, Kayanuma M, Planchat A, Szuwarski N, Blart E, Pellegrin Y, Daniel C, Boujtita M and Odobel F 2013 First application of the HETPHEN concept to new heteroleptic bis(diimine) copper(I) complexes as sensitizers in dye sensitized solar cells *Dalton Trans.* **42** 10818–27
- [66] Cuttall D G, Kuang S M, Fanwick P E, McMillin D R and Walton R A 2002 Simple Cu(I) complexes with unprecedented excited-state lifetimes *J. Am. Chem. Soc.* **124** 6–7
- [67] Hsu C W, Lin C C, Chung M W, Chi Y, Lee G H, Chou P T, Chang C H and Chen P Y 2011 Systematic investigation of the metal-structure-photophysics relationship of emissive d<sup>10</sup>-complexes of group 11 elements: The prospect of application in organic light emitting devices *J. Am. Chem. Soc.* **133** 12085–99
- [68] Vorontsov I I, Graber T, Kovalevsky A Y, Novozhilova I V, Gembicky M, Chen Y S and Coppens P 2009 Capturing and analyzing the excited-state structure of a Cu(I) phenanthroline complex by time-resolved diffraction and theoretical calculations *J. Am. Chem. Soc.* **131** 6566–73
- [69] Tschierlei S, Karnahl M, Rockstroh N, Junge H, Beller M and Lochbrunner S 2014 Substitution-controlled excited state processes in heteroleptic copper(I) photosensitizers used in hydrogen evolving systems *ChemPhysChem* **15** 3709–13
- [70] Iwamura M, Takeuchi S and Tahara T 2007 Real-time observation of the photoinduced structural change of bis(2,9-dimethyl-1,10-phenanthroline)copper(I) by femtosecond fluorescence spectroscopy: A realistic potential curve of the Jahn–Teller distortion *J. Am. Chem. Soc.* **129** 5248–56
- [71] Iwamura M, Watanabe H, Ishii K, Takeuchi S and Tahara T 2011 Coherent nuclear dynamics in ultrafast photoinduced structural change of bis(diimine)copper(I) complex *J. Am. Chem. Soc.* **133** 7728–36
- [72] Fischer S *et al* 2014 Death and rebirth: Photocatalytic hydrogen production by a self-organizing copper-iron system *ACS Catal.* **4** 1845–9
- [73] Heberle M, Tschierlei S, Rockstroh N, Ringenberg M, Frey W, Junge H, Beller M, Lochbrunner S and Karnahl M 2017 Heteroleptic copper photosensitizers: why an extended  $\pi$ -system does not automatically lead to enhanced hydrogen production *Chem. Eur. J.* **23** 312–9
- [74] Cannizzo A, Van Mourik F, Gawelda W, Zgrabcic G, Bressler C and Chergui M 2006 Broadband femtosecond fluorescence spectroscopy of [Ru(bpy)<sub>3</sub>]<sup>2+</sup> *Angew. Chem., Int. Ed. Engl.* **45** 3174–6
- [75] Hedley G J, Ruseckas A and Samuel I D W 2009 Ultrafast intersystem crossing in a red phosphorescent iridium complex *J. Phys. Chem. A* **113** 2–4
- [76] Chergui M 2012 On the interplay between charge, spin and structural dynamics in transition metal complexes *Dalton Trans.* **41** 13022–9
- [77] Schulz M, Reichardt C, Müller C, Schneider K R A, Holste J and Dietzek B 2017 Excited state properties of heteroleptic Cu(I) 4*H*-imidazolate complexes *Inorg. Chem.* **56** 12978–86
- [78] Garakyaraghi S, Danilov E O, McCusker C E and Castellano F N 2015 Transient absorption dynamics of sterically congested Cu(I) MLCT excited states *J. Phys. Chem. A* **119** 3181–93
- [79] Juban E A, Smeigh A L, Monat J E and McCusker J K 2006 Ultrafast dynamics of ligand-field excited states *Coord. Chem. Rev.* **250** 1783–91
- [80] Cannizzo A, Milne C J, Consani C, Gawelda W, Bressler C, van Mourik F and Chergui M 2010 Light-induced spin crossover in Fe(II)-based complexes: The full photocycle unraveled by ultrafast optical and x-ray spectroscopies *Coord. Chem. Rev.* **254** 2677–86
- [81] Auböck G and Chergui M 2015 Sub-50-fs photoinduced spin crossover in [Fe(bpy)<sub>3</sub>]<sup>2+</sup> *Nat. Chem.* **7** 629–33
- [82] McCusker J K, Rheingold A L and Hendrickson D N 1996 Variable-temperature studies of laser-initiated  ${}^5T_2 \rightarrow {}^1A_1$  intersystem crossing in spin-crossover complexes: Empirical correlations between activation parameters and ligand structure in a series of polypyridyl ferrous complexes *Inorg. Chem.* **35** 2100–12
- [83] Liu Y, Persson P, Sundström V and Wärnmark K 2016 Fe *N*-heterocyclic carbene complexes as promising photosensitizers *Acc. Chem. Res.* **49** 1477–85
- [84] Duchanois T, Etienne T, Cebrián C, Liu L, Monari A, Beley M, Assfeld X, Haacke S and Gros P C 2015 An iron-based photosensitizer with extended excited-state lifetime:



- photophysical and photovoltaic properties *Eur. J. Inorg. Chem.* **2015** 2469–77
- [85] Liu L, Duchanois T, Etienne T, Monari A, Beley M, Assfeld X, Haacke S and Gros P C 2016 A new record excited state <sup>3</sup>MLCT lifetime for metalorganic iron(II) complexes *Phys. Chem. Chem. Phys.* **18** 12550–6
- [86] Harlang T C B *et al* 2015 Iron sensitizer converts light to electrons with 92% yield *Nat. Chem.* **7** 883–9
- [87] Liu Y *et al* 2015 A heteroleptic ferrous complex with mesoionic bis(1,2,3-triazol-5-ylidene) ligands: Taming the MLCT excited state of iron(II) *Chem. Eur. J.* **21** 3628–39
- [88] Steube J, Burkhardt L, Pöpcke A, Moll J, Zimmer P, Schoch R, Wölper C, Heinze K, Lochbrunner S and Bauer M 2019 Excited state kinetics of an air-stable cyclometalated iron(II) complex *Chem. A Eur. J.* **25** 11826–30
- [89] Chábera P *et al* 2017 A low-spin Fe(III) complex with 100-ps ligand-to-metal charge transfer photoluminescence *Nature* **543** 695–9
- [90] Kjær K S *et al* 2019 Luminescence and reactivity of a charge-transfer excited iron complex with nanosecond lifetime *Science* **363** 249–53
- [91] Rosas-Hernández A, Steinlechner C, Junge H and Beller M 2018 Photo- and electrochemical valorization of carbon dioxide using earth-abundant molecular catalysts *Top. Curr. Chem.* **376** 229–53
- [92] Debye P 1942 Reaction rates in ionic solutions *J. Electrochem. Soc.* **82** 265–72
- [93] Günther J P, Majer G and Fischer P 2019 Absolute diffusion measurements of active enzyme solutions by NMR *J. Chem. Phys.* **150** 124201
- [94] Mejía E, Luo S P, Karnahl M, Friedrich A, Tschierlei S, Surkus A E, Junge H, Gladiali S, Lochbrunner S and Beller M 2013 A noble-metal-free system for photocatalytic hydrogen production from water *Chem. Eur. J.* **19** 15972–8
- [95] Straub S, Brünker P, Lindner J and Vöhringer P 2018 An iron complex with a bent, O-coordinated CO<sub>2</sub> ligand discovered by femtosecond mid-infrared spectroscopy *Angew. Chem. Int. Ed.* **57** 5000–5